Gap solitons in a medium with third-harmonic generation

Richard S. Tasgal and Y. B. Band

Departments of Chemistry and Electro-Optics, Ben-Gurion University of the Negev, Beer-Sheva 84105, Israel

Boris A. Malomed

Department of Interdisciplinary Studies, School of Electrical Engineering, Faculty of Engineering, Tel Aviv University, Tel Aviv 69978, Israel

We find two-component optical solitons in a nonlinear waveguide with a Bragg grating, including Kerr effects and third-harmonic generation (THG). The model may be realized in temporal and in spatial domains. Two species of fundamental gap solitons (GSs) are found. The first ("THG-gap soliton") has the bulk of its energy at the fundamental frequency (FF) and a lesser part in the third-harmonic (TH) band. The FF part of the soliton is always single humped; the TH part may be single or double humped. Stability domains for quiescent and moving THG-gap solitons strongly shrink with increase of velocity. The second species is the usual ("simple") GS, sitting entirely in the TH band. More complex solutions are also found, in the form of a bound state of a THG-gap soliton and two simple GSs, with a finite binding energy. When a THG-gap soliton is unstable, the instability is oscillatory. It may ultimately cause the THG-gap soliton to throw off some radiation and evolve into a localized structure with the FF and TH components out of phase, with or without internal oscillations. Stable solitons feature an excited state (i.e., they support a localized eigenmode).

I. INTRODUCTION

Gap solitons (GSs) in temporal [1–3] and spatial [4] domains have been predicted in nonlinear media with Bragg gratings (BGs). The BG creates (in the temporal domain) dispersion or (in the spatial domain) diffraction, which, in combination with material nonlinearity, supports GSs. GSs have been the focus of much research due to potential applications, and because they are one of only a few distinct basic soliton types (see earlier [5] and more recent [6] reviews of GSs). A crucially important property of a resonant BG (i.e., modulation of the index of refraction at a period that is in-phase with the wavelength of the light) is that the group-velocity dispersion (or, in the spatial domain, diffraction) induced by the Bragg scattering can be several orders of magnitude larger than the intrinsic material (geometric) dispersion (diffraction) of the homogeneous optical medium. As a consequence, GSs may be realized at much shorter lengths than nonlinear Schrödinger (NLS) solitons [7]—in the temporal domain, GSs are typically on the order of centimeters long, while NLS solitons are generally kilometers. Temporal-domain GSs have been produced in fiber gratings less than 10 cm long [8–10]. Recently, spatial GSs have been observed in waveguide arrays [11] and in photonic lattices induced in a photorefractive material [12]. Besides the Kerr nonlinearity in the original GS work, GSs have been predicted in systems combining a BG with other optical nonlinearities, such as second-harmonic generation (SHG) [13], self-induced transparency [14], and a combination of self-focusing cubic and self-defocusing quintic terms [15]. Also, more complicated types of spatial GSs, but with a simple cubic ($\chi^{(3)}$) nonlinearity, have been predicted [16].

There has been a particularly significant interest in *two-color* GSs supported by SHG ($\chi^{(2)}$ nonlinearity) and Bragg gratings [17]. However, despite the theoretical predictions, two-color GSs have not yet been experimentally created, either in the temporal or the spatial domain. The problem is obvious, it is hard to fabricate a long waveguide or fiber from quadratic materials (a SHG monocrystal or a periodically poled medium) and also to write a regular grating on it. The situation is especially problematic for temporal solitons, as SHG waveguides are in practice, even without the added difficulty of creating a BG on the waveguide, limited to a few centimeters. Thus for SHG solitons, the nonlinear length and the dispersion length of the soliton (at both harmonics) must both be no larger than about 1 cm, which is extremely difficult.

There has been much research that partly overlaps with the model we propose. Ordinary (without a BG-induced band gap) two-color solitons supported by a SHG nonlinearity have been thoroughly investigated theoretically in myriad settings (see, e.g., Ref. [18]). They have been created experimentally in the spatial domain (see Ref. [19]). A temporal-domain $\chi^{(2)}$ soliton was observed in Ref. [20]. The latter demanded a special effort to avoid the problem of insufficient material group-velocity dispersion—creating additional effective dispersion with the tilted wavefront technique in a planar geometry. Ordinary (without a BG-induced band gap) two-color temporal solitons supported by the nonlinearities THG and Kerr effects [self- and cross-phase modulation (SPM, XPM)] were predicted in Ref. [21]. These two-color solitons are far from experimental realization for a number of reasons, the most serious being the lack of tools to enforce phase- and group-velocity matching between the fundamental frequency (FF) and third harmonic (TH) bands. In other words, THG, while it occurs *locally*, is washed out due to a large phase-velocity mismatch [see Ref. [22], where numerical simulations of the full system of Maxwell's equations with a cubic nonlinearity, including both instantaneous

(SPM, XPM, and THG) and retarded (Raman) effects, were performed]. Recently, solitons were considered in models combining a nonlinearly induced grating and THG [23]. (Note that this is very different from a system with a linear BG, as in the present work. See Ref. [24] for solitons in a system with a nonlinearly induced grating, but no THG.) From yet another direction—not solitons, but rather towards the goal of producing significant THG—various means of attaining phase-matching between FF and TH waves have recently been analyzed, for example, photonic crystals [25] and use of the Kerr effect [26]. The strong dispersion provided by a BG, which may be a most effective tool for tuning FF and TH waves, has not been considered in this nonsoliton context either.

In this work, we propose a way of making (temporal or spatial) two-color GSs, using third-harmonic generation (THG) rather than SHG. This approach is more realizable, as one does not need to manufacture a fiber (or waveguide) from $\chi^{(2)}$ materials, which are difficult to work with. Experimental realization requires the same sort of waveguide as for simple GSs [8–10], with the additional stipulation that it must be sufficiently nonabsorbent at the TH as well as at the FF (over the relevant propagation length). An ordinary dielectric medium with a Kerr nonlinearity ($\chi^{(3)}$), such as silica or AlGaAs (which has a nonlinear coefficient approximately 500 times larger than silica, making the necessary lengths much smaller) will do the job. Current technology can readily produce regular gratings more than a meter long on such materials by writing the BG on the fiber cladding—this is more than long enough for GS experiments [8–10]. Another way to realize the system is with a photonic-crystal fiber with a hollow core—here, the BG can be written on the inner surface of the fiber, as proposed in, e.g, Ref. [27]. The condition of nonabsorption (over the relevant length) is relatively lax because the relevant length for GSs is quite small. For propagation lengths up to about 1 m, sufficiently low fiber loss at the fundamental frequency and third-harmonic bands is easily achieved in optical fibers. A comparison with typical experimentally realizable simple GSs [8–10] suggests that solitons in the THG-Bragg grating system will have spatial extent $\lesssim 1$ cm, peak power density on the order of 10 GW/cm^2, and (if the GS is produced in a straightforward experiment by simple self-trapping of a soliton from a laser pulse) soliton velocity between $c/(2n)$ and c/n, where c is the speed of light in vacuum and n is the mean index of refraction in the fiber. The combination of THG and Kerr nonlinearity with a BG thus offers a real possibility of creating two-color gap solitons, which may be practically unattainable by other means.

In Sec. II, we set forward a model for light in a waveguide with a BG (in resonance with both the FF and TH waves), and with SPM, XPM, and THG nonlinearities. The model applies to light evolution in both temporal and spatial domains in $\chi^{(3)}$ media. The relaxation method, by which we find numerical soliton solutions, is briefly described in the Appendix. Section III characterizes quiescent (zero-velocity) fundamental and compound solitons in detail. The set of fundamental solitons include "simple" ones, with only the TH component present, which are equivalent to the simple GSs [1–3], and a family of two-color THG-gap solitons. Most of

the solutions are found to be stable. A feature of the THG-gap soliton (not exhibited by the simple GSs) is that they may feature both single-humped and double-humped shapes in the TH component, and the soliton may be stable in both cases. Solitons with several humps in the FF band, which may be considered as compound solitons, i.e., stable bound states comprised of one THG-gap soliton and two simple GSs in the TH, are also found. The existence and stability of such compound objects is a noteworthy result, as they are absent in the standard BG model. Moving THG-gap solitons are considered in Sec. IV (in the spatial domain model, the "moving" solitons represent tilted beams in the planar waveguide). Detailed discussion of the solitons' stability is presented in Sec. V. A feature of THG-gap solitons is that the stability region quickly shrinks with the increase of the velocity, and all the moving solitons become unstable when the velocity attains a critical value (which is, roughly, half-the-maximum velocity up to which the solitons exist); this is quite different than simple GSs, for which the stability properties are relatively insensitive to soliton velocity. Section VI concludes the paper.

II. THE MODEL

Propagation of forward- and backward-moving FF and TH waves (at frequencies ω_1 and $3\omega_1$, respectively) in a single-mode lossless waveguide, with a Bragg grating in resonance with the FF and TH, is described by a set of nonlinear coupled-mode equations. Using standard techniques [7,28,29], we derive the equations for the slowly varying envelopes (SVEs) U_1, V_1, U_3, V_3 of which the electric field $E(\mathbf{x}, t)$ is composed,

$$0 = iU_{1,z} + i\delta_1 U_{1,t} + \kappa_1 V_1 + \frac{2\pi(\omega_1/c)^2}{k_1 A_1} 3\chi^{(3)}[(|U_1|^2 + 2|V_1|^2$$
$$+ 2|U_3|^2 + 2|V_3|^2)U_1 + U_1^{*2}U_3], \qquad (1a)$$

$$0 = -iV_{1,z} + i\delta_1 V_{1,t} + \kappa_1^* U_1 + \frac{2\pi(\omega_1/c)^2}{k_1 A_1} 3\chi^{(3)}[(2|U_1|^2 + |V_1|^2$$
$$+ 2|U_3|^2 + 2|V_3|^2)V_1 + V_1^{*2}V_3], \qquad (1b)$$

$$0 = iU_{3,z} + i\delta_3 U_{3,t} + (k_3 - 3k_1)U_3 + \kappa_3 V_3 + \frac{2\pi(3\omega_1/c)^2}{(3k_1)A_3} 3\chi^{(3)}$$
$$\times \left[(2|U_1|^2 + 2|V_1|^2 + |U_3|^2 + 2|V_3|^2)U_3 + \frac{1}{3}U_1^3 \right], \qquad (1c)$$

$$0 = -iV_{3,z} + i\delta_3 V_{3,t} + (k_3 - 3k_1)V_3 + \kappa_3^* U_3 + \frac{2\pi(3\omega_1/c)^2}{(3k_1)A_3} 3\chi^{(3)}$$
$$\times \left[(2|U_1|^2 + 2|V_1|^2 + 2|U_3|^2 + |V_3|^2)V_3 + \frac{1}{3}V_1^3 \right], \qquad (1d)$$

where t and z are time and the coordinate along the waveguide (fiber), subscripts z and t after a comma stand for respective partial derivatives, and asterisk means complex conjugation. Equations (1a) and (1b) govern the evolution of

U_1 and V_1, which are SVEs centered about carrier waves with frequency ω_1 and wave vectors $\pm k_1$ (i.e., forward- and backward-moving FF waves), respectively. Equations (1c) and (1d) are for U_3 and V_3, which are SVEs centered about carrier waves with frequency $3\omega_1$ and wave vectors $\pm 3k_1$ (in other words, they are forward- and backward-moving TH waves). Linear properties of the waveguide with a BG are characterized by the dispersion relation $k = k(\omega) \equiv n(\omega)\omega/c$, where $n(\omega)$ is the refractive index: The wave numbers of the carrier frequencies are $k_1 \equiv k(\omega_1)$ and $\pm 3k_1$. (We choose wave vector $3k_1$ for the carrier wave of the TH SVEs rather than $k_3 \equiv k(3\omega_1)$ so that the phase-velocity mismatch is expressed as an additive linear term rather than as a phase in the THG and parametric downshifting terms [30].) The reciprocal group velocities are $\delta_1 \equiv (dk/d\omega)_{\omega=\omega_1}$ and $\delta_3 \equiv (dk/d\omega)_{\omega=3\omega_1}$. The Bragg reflectivity, assumed frequency-independent within the FF and TH bands, is denoted by κ_1 and κ_3. The well-known condition justifying the latter assumption is that the spatial scale of the field envelopes $U_{1,3}, V_{1,3}$ should be much larger than the period of the Bragg grating and the wavelengths of light. These conditions hold for all cases of practical relevance. The coefficients of the nonlinear terms, SPM, XPM, THG, and the FWM term (i.e., the parametric down-conversion counterpart to THG) are locked together, as in the usual model with an instantaneous nonlinear dielectric response, $P_{NL}(\mathbf{x},t) = \chi^{(3)}[E(\mathbf{x},t)]^3$, where $E(\mathbf{x},t)$ is the whole electric field [7,29]. The cross-sectional areas of the waveguide for the FF and TH waves are A_1 and A_3 [7,28]; setting $A_1 = A_3 = 1$ recovers the equations for plane waves. We have not written coefficients for effects related to the difference in the cross-sectional areas of the fundamental and TH, consequently making the XPM coefficients exactly twice their SPM counterparts. Material dispersion, which is dwarfed by the BG-induced dispersion (typically, by six orders of magnitude) is omitted.

The system of equations (1) can also describe propagation of the forward-backward FF-TH wave quartet in the spatial domain if the variables are identified with other physical quantities. In this case, the forward-backward FF-TH wave quartet propagates in a spatial BG, a system of parallel grooves on a planar waveguide. Waves of the same frequency propagate at the same angle relative to the BG. The variable t, the propagation coordinate, runs parallel to the grooves of the waveguide, z is the perpendicular coordinate, and Δk [see Eq. (4b), below] is a wave vector mismatch. Therefore, the results herein may also represent spatial solitons.

The variables in the governing equations (1) are rescaled,

$$u_1 \equiv U_1 \sqrt{\frac{6\pi(\omega_1/c)^2\chi^{(3)}}{k_1 A_1 \kappa_1}}, \tag{2a}$$

$$v_1 \equiv V_1 \sqrt{\frac{6\pi(\omega_1/c)^2\chi^{(3)}}{k_1 A_1 \kappa_1^*}}, \tag{2b}$$

$$u_3 \equiv U_3 \sqrt{\frac{6\pi(\omega_1/c)^2\chi^{(3)}}{k_1 A_1 \kappa_1^2/\kappa_1^*}}, \tag{2c}$$

$$v_3 \equiv V_3 \sqrt{\frac{6\pi(\omega_1/c)^2\chi^{(3)}}{k_1 A_1 \kappa_1^{*2}/\kappa_1}}, \tag{2d}$$

$$\tau \equiv \frac{|\kappa_1|}{\delta_1}t, \tag{2e}$$

$$\zeta \equiv |\kappa_1|z, \tag{2f}$$

to yield the coupled-mode equations in the normalized form,

$$0 = iu_{1,\tau} + iu_{1,\zeta} + v_1 + (|u_1|^2 + 2|v_1|^2 + 2|u_3|^2 + 2|v_3|^2)u_1 + u_1^{*2}u_3, \tag{3a}$$

$$0 = iv_{1,\tau} - iv_{1,\zeta} + u_1 + (2|u_1|^2 + |v_1|^2 + 2|u_3|^2 + 2|v_3|^2)v_1 + v_1^{*2}v_3, \tag{3b}$$

$$0 = i\delta u_{3,\tau} + iu_{3,\zeta} + \Delta k u_3 + \kappa v_3 + \gamma[3(2|u_1|^2 + 2|v_1|^2 + |u_3|^2 + 2|v_3|^2)u_3 + u_1^3], \tag{3c}$$

$$0 = i\delta v_{3,\tau} - iv_{3,\zeta} + \Delta k v_3 + \kappa^* u_3 + \gamma[3(2|u_1|^2 + 2|v_1|^2 + 2|u_3|^2 + |v_3|^2)v_3 + v_1^3], \tag{3d}$$

with coefficients

$$\delta = \frac{\delta_3}{\delta_1}, \tag{4a}$$

$$\Delta k = \frac{k_3 - 3k_1}{|\kappa_1|}, \tag{4b}$$

$$\kappa = \frac{\kappa_1^* \kappa_3}{\kappa_1^2}, \tag{4c}$$

$$\gamma = \frac{A_1}{A_3}. \tag{4d}$$

Thus, recalling the descriptions of the coefficients above, δ is a ratio of the group velocities, Δk is a dimensionless phase-velocity mismatch, κ is a dimensionless Bragg scattering coefficient, and the Kerr coefficient γ is a ratio of cross-sectional areas of the waveguide modes at the FF and TH. In terms of the dimensionless variables, the FF frequency gap has size $\omega_{gap}(FF) = 2$, and is centered at the middle of the FF frequency band; the TH gap has size $\omega_{gap}(TH) = 2|\kappa/\delta|$, with offset $(\Delta k/\delta)$ from the middle of the TH band.

Equations (3) have three dynamical invariants, one is

$$E_{tot}(\tau) \equiv \int_{-\infty}^{\infty} \left[|u_1|^2 + |v_1|^2 + \frac{\delta}{\gamma}(|u_3|^2 + |v_3|^2) \right] d\zeta, \tag{5}$$

which we refer to as the total energy (in the temporal domain model, it is proportional to the physical energy; in the spatial domain it measures the total power carried by light in the planar waveguide); two others are the Hamiltonian and momentum, which we do not write explicitly. To limit the presentation to a reasonable case with a tractable number of free

parameters, from this point forward we fix the relative group velocity, Bragg and nonlinear coefficients to be $\delta = \kappa = \gamma = 1$. In fact, calculations were also carried out for values of these parameters different from 1; this variation yielded no notable difference in the results. Below, we vary the normalized phase-velocity mismatch Δk (which is known to be the most critical parameter in harmonic-generation systems), and frequencies and velocities of the soliton solutions, as variation of these parameters produces the most interesting results for solitons.

Solutions to Eqs. (3) with a fixed shape and constant velocity (ρ) in both the FF and TH bands were sought in the form

$$u_m(\tau, \zeta) = \exp(-im\omega\tau)u_m(\zeta - \rho\tau), \tag{6a}$$

$$v_m(\tau, \zeta) = \exp(-im\omega\tau)v_m(\zeta - \rho\tau), \tag{6b}$$

with $m = 1$ and $m = 3$. This simply says that the solutions should be of fixed shape, with constant eigenvalue and velocity. Substituting this *ansatz* into Eqs. (3) yields a set of ordinary differential equations whose localized solutions are solitons. The numerical procedure used to solve the latter set of equations is described in the Appendix.

III. FUNDAMENTAL THG-GAP SOLITONS

An obvious family of solitons has all the energy in the TH ($u_3, v_3 \not\equiv 0$) and nothing in the FF band ($u_1 = v_1 = 0$). In this case, Eqs. (3c) and (3d) for the TH components u_3, v_3 reduce to those for simple GSs, whose soliton solutions [2,3] and stability properties [32,33] are known (an additional linear instability of these solitons cannot be induced by small perturbations in the FF band, as their coupling to the TH equations is nonlinear). We refer to them as Aceves-Wabnitz-Christodoulides-Joseph (AWCJ) solitons. Direct simulations (not shown here) demonstrate that the coupling to the FF fields does not add a nonlinear instability to the AWCJ solitons in the TH component either.

The second family of solutions, which we will refer to as THG-gap solitons, are qualitatively distinct. In the regions examined herein, they have the bulk of their energy in the FF component, and a smaller amount in the TH band. The THG-gap solitons were found to always display a single-humped shape in the FF band, while their shape in the TH components may be either single or double humped. Figures 1 and 2 illustrate a single-humped quiescent ($\rho = 0$) THG-gap soliton (Fig. 1 shows it in coordinate space, and Fig. 2 in wave number space). Figures 3 and 4 illustrate a quiescent THG-gap soliton with a double-humped structure in the TH band (Fig. 3 in coordinate space, and Fig. 4 in wave number space).

We found THG-gap solitons in a two-dimensional region in parameter space, shown in Fig. 5. Obvious existence conditions for the THG-gap solitons are $|\omega|, |3\omega + \Delta k| < 1$, meaning that the solitons must sit inside the band gaps in each component; outside this region, the solutions become delocalized. Close to other borders, the THG-gap soliton may be lost by becoming singular through developing too many high
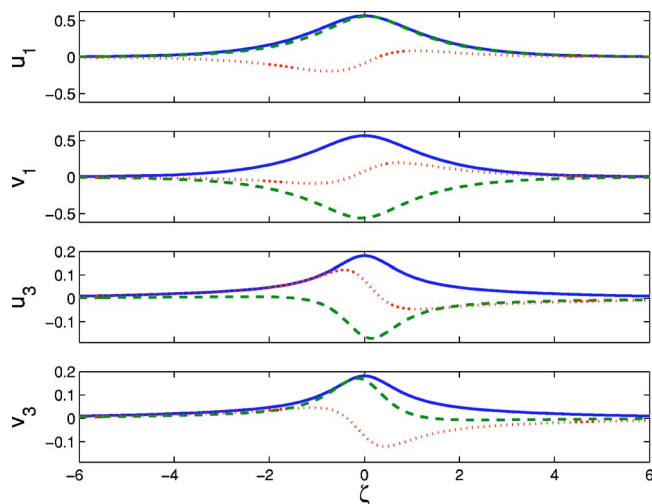

FIG. 1. (Color online) Typical example of a quiescent ($\rho = 0$) THG-gap soliton with the single-humped structure, in the coordinate space. The solution has $\omega = 0.52$ and $\Delta k = -2.09$. Here and in Fig. 3 below, the solid, dashed, and dotted lines show, respectively, the absolute value, real, and imaginary parts of the four constituent fields.

wave numbers. However, the evidence provided by the relaxation method close to the borders is insufficient to remove ambiguity about the cause.

A fundamental characteristic of the family of THG-gap solitons is that, like the AWCJ solitons, all the quiescent ($\rho = 0$) solitons satisfy symmetry restrictions that are compatible with the corresponding equations, $u(\zeta) = -v(-\zeta)$ and $u(\zeta) = -v^*(\zeta)$. Figure 6 shows the total energy of the family of the THG-gap solitons, E_{tot} vs ω and Δk, within the existence region of the solitons. Note that, for any fixed phase-velocity mismatch Δk, the energy E_{tot} decreases as a function of the FF frequency ω. By the Vakhitov-Kolokolov criterion [34], this implies that the quiescent THG-gap solitons cannot be unstable against nonoscillatory perturbations (corresponding to real unstable eigenvalues).
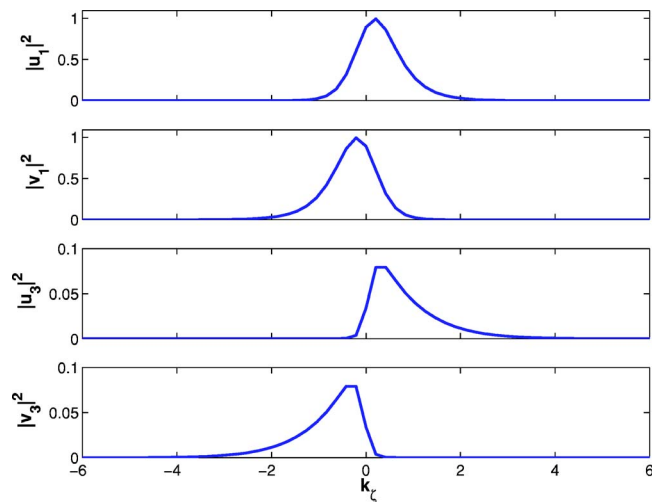

FIG. 2. (Color online) Fourier image of the THG-gap soliton from Fig. 1. The power spectrum (absolute square) of the solution is displayed.
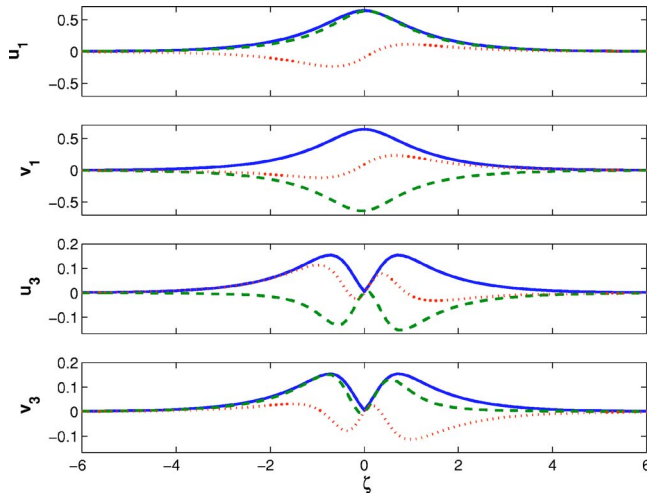
FIG. 3. (Color online) Typical example of a quiescent ($\rho=0$) THG-gap soliton featuring a double-humped structure in its TH component in the coordinate space, found at $\omega=0.38$ and $\Delta k=-1.47$.

Figure 7 shows the share of the soliton's energy in its TH component, $\int_{-\infty}^{+\infty}(|u_3|^2+|v_3|^2)d\zeta/E_{\text{tot}}$ vs the same parameters, ω and Δk, and Fig. 8 displays the "cleavage depth" in the TH component, $M(\tau)\equiv(|u_3(\tau,0)|^2+|v_3(\tau,0)|^2)/\max_\zeta(|u_3(\tau,\zeta)|^2+|v_3(\tau,\zeta)|^2)$. A value $M=1$ means that the TH component of the soliton is single humped, while $M<1$ indicates a double-humped structure. Figure 5 shows that a large region of the single-humped solitons is adjacent to a region with a deep cleavage, which is followed by a region with a more moderate drop-off of the intensity between the humps.

Compound THG-gap solitons: We have also found a family of solitons with multiple humps in the FF. We refer to these as compound solitons, since they may be considered as bound states of THG-gap solitons and simple AWCJ ones. A typical example is displayed in Fig. 9. This particular solution continues, in parameter space, into a family of compound solitons. To illustrate the family and compare it with
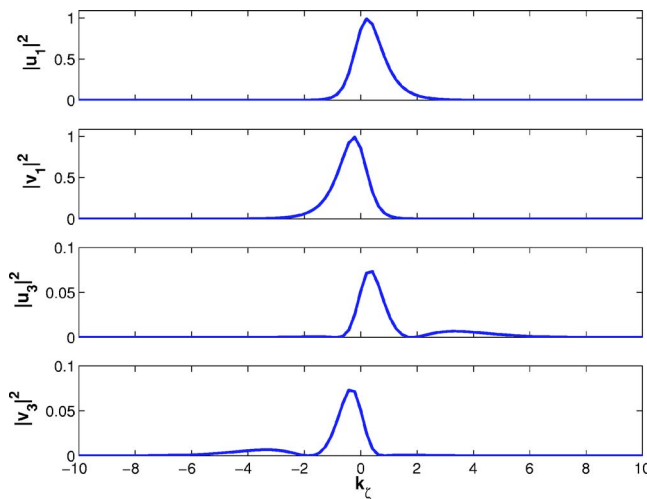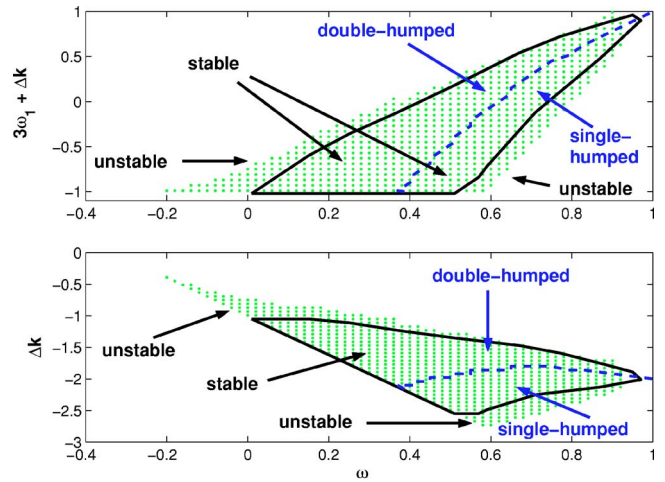

FIG. 5. (Color online) Regions of existence (dots) and stability (bounded by the solid lines), and shape of the third-harmonic component (single- and double-humped regions separated by a dashed line) for quiescent (zero velocity) THG-gap solitons in the parameter plane $(\omega,3\omega+\Delta k)$, where Δk is phase-velocity mismatch, and ω is FF frequency; the same for the parameter plane $(\omega,\Delta k)$. Stability was determined by direct numerical simulations, up to $\tau=200$.

families of fundamental solitons, Fig. 10 shows the energies of the THG-gap solitons, AWCJ solitons, and compound ones over a range of FF frequencies ω, for a fixed phase-velocity mismatch Δk. The soliton shown in Fig. 9 has three distinct peaks in the TH component (which holds for the entire family originating from this solution), while both the simple AWCJ solitons and the THG-gap ones always feature a single-humped shape in this component. The three distinct peaks in the FF component for this example of a compound soliton do not persist in the entire family of compound soliton solutions—the side FF peaks may sometimes merge into the central one.

A detailed consideration allows us to interpret this compound as a bound state of one THG-gap soliton and two AWCJ solitons. This interpretation motivates a definition of
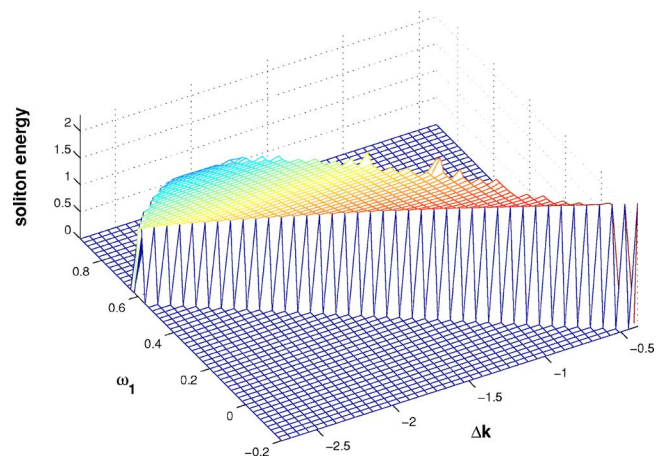

FIG. 4. (Color online) Fourier image of the THG-gap soliton from Fig. 3. The power spectrum (absolute square) is shown.

FIG. 6. (Color online) Energy of the THG-gap soliton, defined as per Eq. (5), over the soliton's existence region, as a function of phase-velocity mismatch Δk and frequency ω.
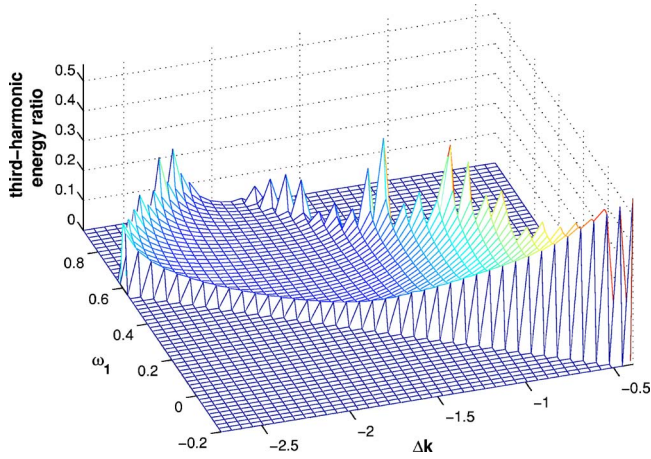
FIG. 7. (Color online) Share of the THG-gap soliton's energy in the third-harmonic component. The data are displayed over the soliton's existence region in parameter space of phase-velocity mismatch Δk and eigenvalue ω.

energy defect (or as a "mass defect" if the conserved quantity E_{tot} is considered as its effective mass; or also as a binding enegy)

$$\Delta E = E_{\text{THG gap}} + 2E_{\text{AWCJ}} - E_{\text{compound}}, \tag{7}$$

as a combination of the respective energies, each computed separately according to Eq. (5) at the same values of ω and Δk. Results are shown in Fig. 11. The positive definite energy defect implies that the compound soliton should be stable, which is always confirmed by direct simulations (not shown here).

IV. MOVING THG-GAP SOLITONS

We performed systematic searches for moving THG-gap solitons over two dimensions in the parameter space, soliton
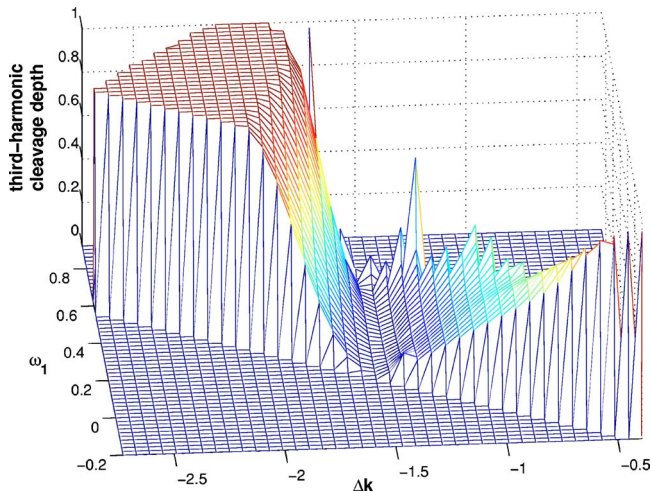

FIG. 8. (Color online) Cleavage depth of the THG-gap soliton in its third-harmonic component, whose shape may be both single humped and double humped, is shown over its existence region, as a function of phase-velocity mismatch Δk and eigenvalue ω. Values less than unity indicate a double-humped structure in the third-harmonic component.
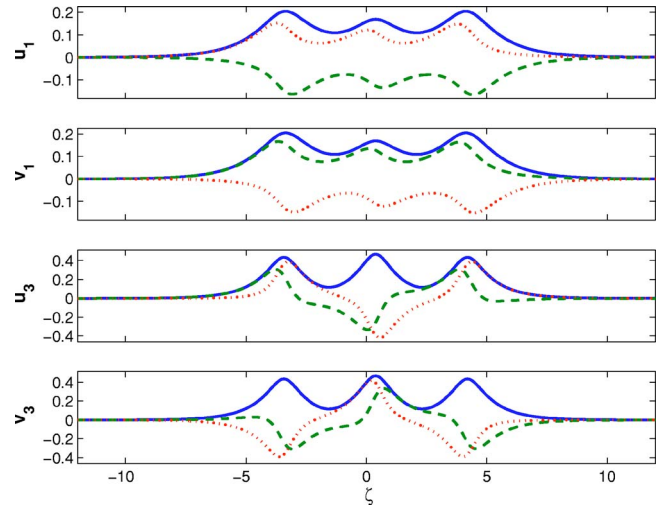

FIG. 9. (Color online) Compound quiescent $(\rho=0)$ THG-gap soliton in the coordinate space, at frequency $\omega=0.58$ and phase-velocity mismatch $\Delta k=-1.89$. The solid, dashed, and dotted lines show the absolute values, real, and imaginary parts of the fields.

velocity ρ and frequency ω [see Eqs. (6)]. To illustrate the generic situation, we present results for a constant phase-velocity mismatch, $\Delta k=-1.89$. Typical examples of moving THG-gap solitons are displayed in Figs. 12 and 13. Clearly, symmetries of the quiescent THG-gap solitons between the forward $u_{1,3}$ and backward $v_{1,3}$ components are broken by a finite velocity.

Figure 14 summarizes numerical results for the moving THG-gap solitons, existence and stability domains in the (ω, ρ) parameter space (cf. Fig. 5 for quiescent solitons). The family of moving solitons is further quantified by Fig. 15, which shows the soliton energy vs velocity and frequency. Note that, as in the case of quiescent solitons, energy always decreases smoothly with the frequency. The disappearance of
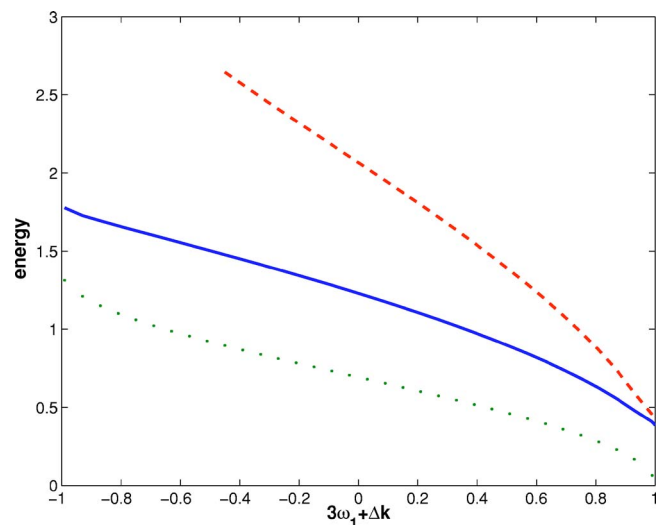

FIG. 10. (Color online) Energy [defined in Eq. (5)] for the THG-gap soliton (solid line), AWCJ soliton (dotted), and the compound soliton (dashed) vs frequency ω, for a fixed phase-velocity mismatch, $\Delta k=-1.89$.
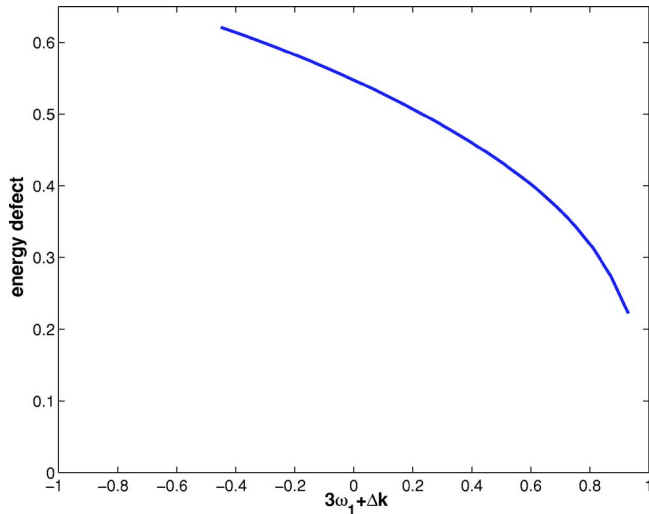
FIG. 11. (Color online) Energy defect (binding energy) of the compound soliton, defined in Eq. (7) vs frequency ω, for fixed phase-velocity mismatch, $\Delta k = -1.89$.

FIG. 13. (Color online) The same as in Fig. 12, but for $\omega = 0.86$ and $\rho = 0.1$. This THG-gap soliton is stable.

the moving solitons at borders of their existence region can, in some cases, be traced to the energy in one of the FF modes approaching zero. Other boundaries of the existence region are harder to interpret, due to poor convergence of the relaxation method very close to the borders. As for quiescent THG-gap solitons, the moving THG-gap soliton may develop a singularity as it approaches the borders. Stable moving compound states can also be found, but we do not display them here.

V. STABILITY

The Vakhitov-Kolokolov (VK) criterion [34], applied to the families of the THG-gap solitons, disallows nonoscilla-

tory instabilities. Full stability of the solitons was investigated by direct numerical simulations, propagating the solution with a small initial perturbation by means of the split-step fast-Fourier-transform method [7]. Stability borders identified this way are shown in Fig. 5 for quiescent THG-gap solitons, and in Fig. 14 for the moving THG-gap solitons. All the soliton instabilities were found to be oscillatory, consistent with the VK criterion precluding monotonic instabilities. A notable characteristic of THG-gap solitons is that their stability region considerably shrinks with increase of the velocity (in sharp contrast to the AWCJ solitons, whose stability depends only weakly on the velocity [33]). The velocity up to which THG-gap solitons remain stable is smaller (roughly, by a factor of 2) than the velocity up to which THG-gap solitons exist.

Figure 16 illustrates, through the evolution of peak intensities of all the fields, propagation of a fairly typical stable
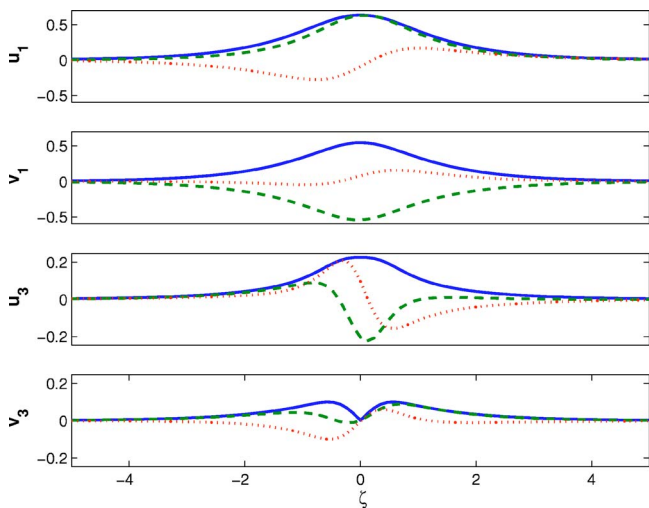

FIG. 12. (Color online) Example of an (unstable) moving THG-gap soliton in the coordinate space, for phase-velocity mismatch $\Delta k = -1.89$, FF frequency $\omega = 0.44$, and velocity $\rho = 0.2$. The solid, dashed, and dotted lines are the absolute values, real parts, and imaginary parts of the amplitudes.
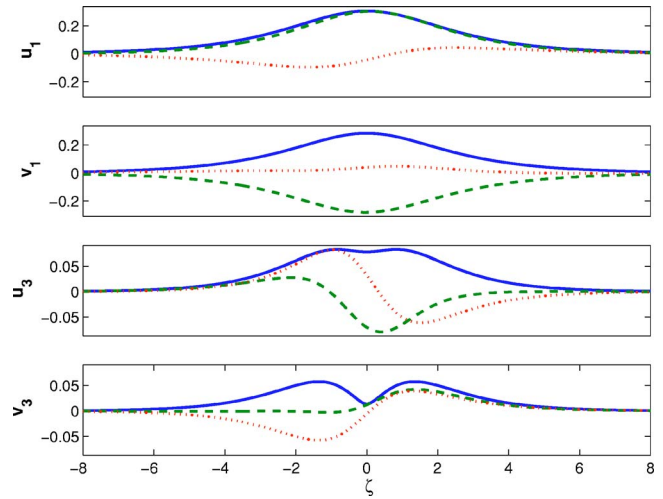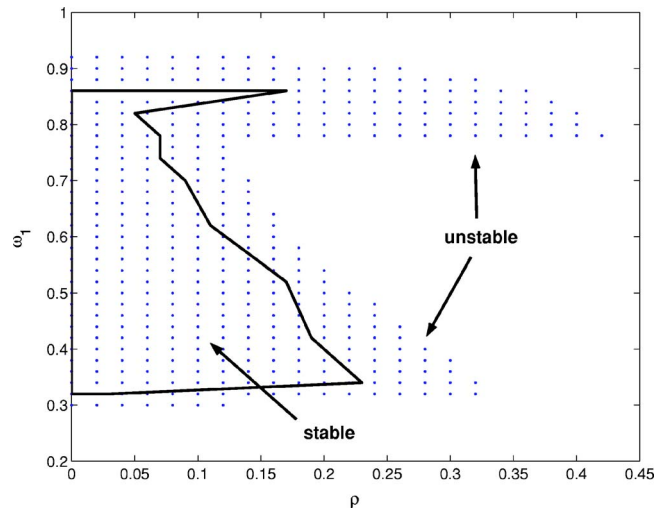

FIG. 14. (Color online) Existence and stability regions for moving THG-gap solitons in the parameter space of velocity and FF frequency, (ρ, ω), for constant phase-velocity mismatch, $\Delta k = -1.89$. Stability was identified by direct simulations, similar to the case of Fig. 5.
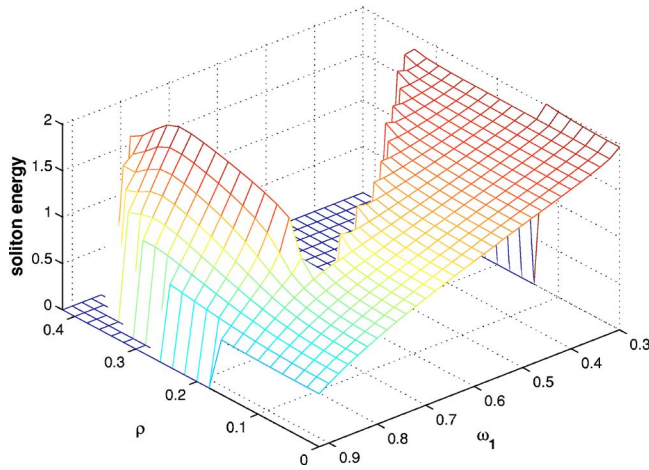
FIG. 15. (Color online) Energy of moving THG-gap solitons [defined as per Eq. (5)] vs velocity ρ and frequency ω, for fixed phase-velocity mismatch, $\Delta k = -1.89$.

THG-gap soliton, to which initial perturbation noise was added. The perturbation does not completely disappear, but rather excites persistent internal vibrations of the soliton. This strongly suggests existence of a stable intrinsic mode.

Figures 17 and 18 illustrate evolution of an initially perturbed unstable THG-gap soliton. In this case, most of the initial noise disperses, but a particular perturbation mode grows and destroys the soliton. The localized pulse does not then disappear, but rather becomes a breather. In this example, as well as in all others observed, the surviving localized structures seem to be mutually incoherent, in the sense that its FF and TH component remain effectively coupled only through the XPM interaction, while the phase-sensitive THG and FWM couplings are virtually nullified by the rapid oscillations. The stability and instability of moving solitons is generally similar to that of their quiescent counterparts.
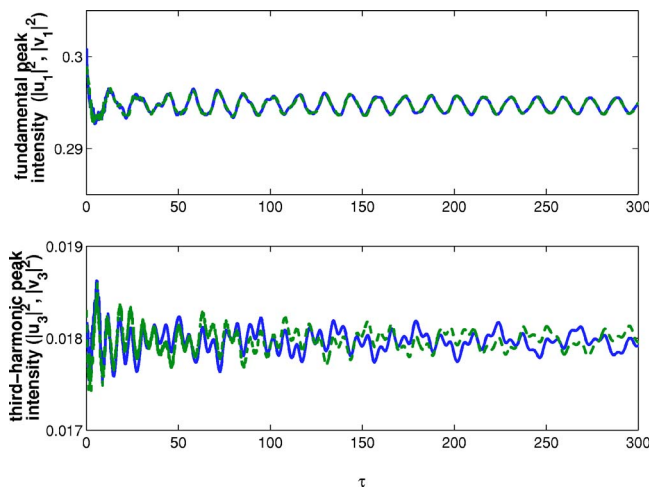

FIG. 16. (Color online) Evolution of the peak intensities of the constituent fields (maximum values of the absolute squares) from a stable perturbed quiescent THG-gap soliton, for phase-velocity mismatch $\Delta k = -2.25$ and FF frequency $\omega = 0.56$. Solid and dashed lines are for, respectively, fields $u_{1,3}$ and $v_{1,3}$. The peak intensities of fields u_1 and v_1 and of u_3 and v_3 are visually indistinguishable.
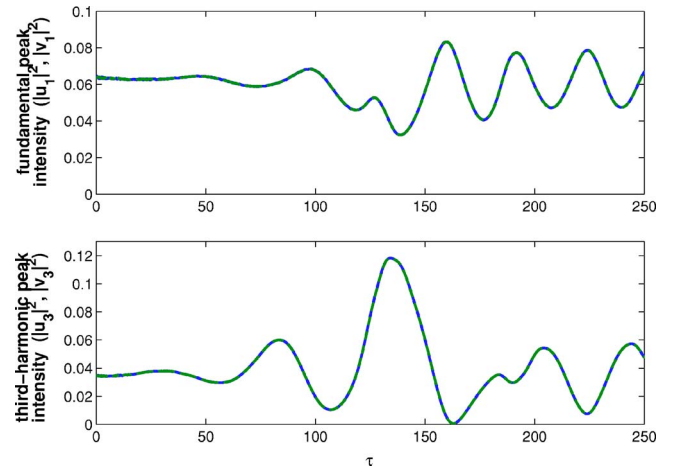

FIG. 17. (Color online) The same as in Fig. 16, but for an unstable THG-gap soliton, with $\Delta k = -2.25$ and $\omega = 0.88$. As in Fig. 16, the intensities of the FF fields u_1 and v_1 and of the TH fields u_3 and v_3 are visually indistinguishable.

Figures 19 and 20 illustrate evolution of all the fields from, initially, an unstable moving THG-gap soliton with noise perturbation. This figure displays the evolution of the peak intensities as a function of time τ, and Fig. 20 displays a surface plot with the field intensities as functions of (ζ, τ). The oscillatory perturbations grow until they destroy the THG-gap soliton, which then evolves into a messier breathing localized state.

VI. CONCLUSIONS

We have introduced a coupled-mode system for the forward- and backward-propagating fundamental frequency (FF) and third-harmonic (TH) waves, which are linearly coupled by a resonant Bragg scattering (on a single Bragg grating), and nonlinearly coupled by a full set of third-order nonlinear ($\chi^{(3)}$) terms, including self- and cross-phase modulation (SPM and XPM), third-harmonic generation (THG), and four-wave mixing (FWM—or, more specifically, the
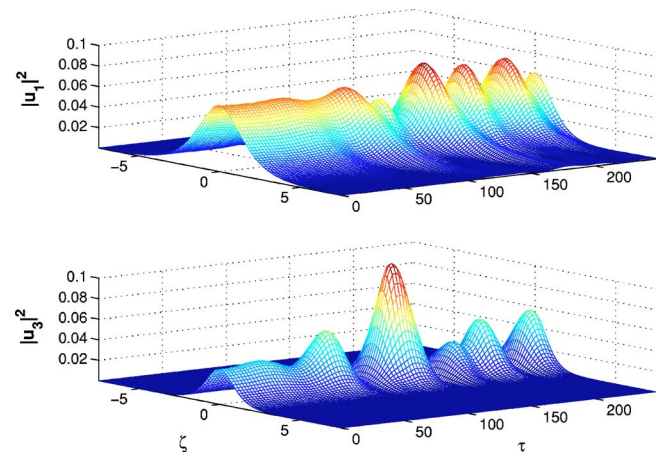

FIG. 18. (Color online) Surface plots of field intensities for the same case as in Fig. 17.
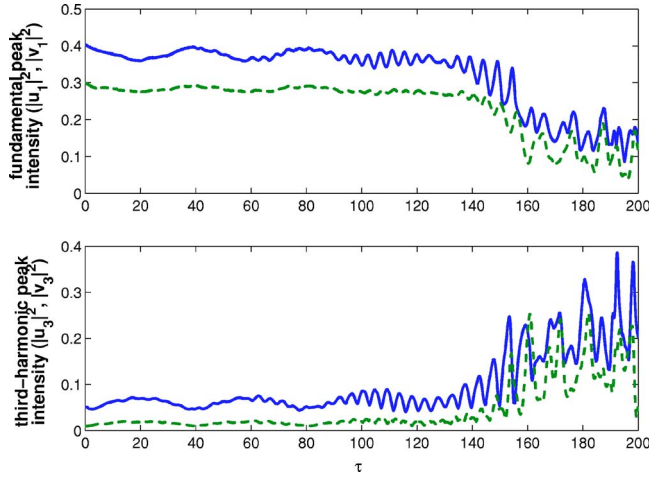
FIG. 19. (Color online) Evolution of the peak intensities of the constituent fields (maximum values of the absolute squares) from an unstable perturbed moving THG-gap soliton, for phase-velocity mismatch $\Delta k = -1.89$, frequency $\omega = 0.44$, and velocity $\rho = 0.2$. Solid and dashed lines are for fields $u_{1,3}$ and $v_{1,3}$, respectively.

parametric downconversion that is an inverse of THG). The model may be realized in both the temporal and spatial domains, i.e., in a fiber (which seems especially interesting), or in a planar waveguide, with an appropriate grating. The model exhibits a variety of soliton behaviors. Alongside the gap solitons (GSs) in the TH band alone [which are identical to (well-known) simple GS solutions], we have found a qualitatively distinct species of "THG-gap" solitons, with energy split between the FF and TH bands. In the better part of the existence region, quiescent (zero-velocity) THG-gap solitons are stable. For moving THG-gap solitons, the stability region quickly shrinks with increase of velocity. The TH component of stable THG-gap solitons may assume both single- and double-humped shapes. (Note that double humps
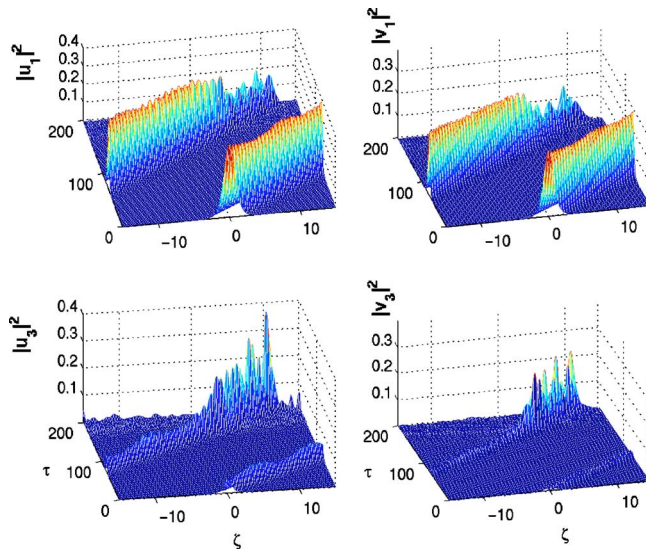

FIG. 20. (Color online) Evolution of the constituent field intensities (squares of the absolute value) from an unstable moving THG-gap soliton, for phase-velocity mismatch $\Delta k = -1.89$, frequency $\omega = 0.44$, and velocity $\rho = 0.2$ (the same case as in Fig. 19).

do not exist in the simple GSs supported by a Bragg grating.) When the THG-gap soliton is unstable, it may evolve, shedding some radiation, into a localized structure, often in the form of a breather. Compound solitons were also found, in the form of bound states of two simple GSs in the TH band and one THG-gap soliton. Stability of the compound solitons was confirmed by calculation of a finite binding energy. Stable THG solitons support an intrinsic mode, i.e., they may exist in an excited state.

The theoretical results reported here suggest experiments which may achieve two purposes that have so far been elusive: creation of two-color GSs, and creation of a soliton combining the fundamental-frequency and third-harmonic waves.

APPENDIX: THE RELAXATION METHOD

Substituting the *ansatz* (6) into the set of partial differential equations (3) yields the set of ordinary differential equations,

$$0 = \omega u_1 + i(1-\rho)u_1' + v_1 + (|u_1|^2 + 2|v_1|^2 + 2|u_3|^2 + 2|v_3|^2)u_1$$
$$+ u_1^{*2}u_3, \tag{A1a}$$

$$0 = \omega v_1 - i(1+\rho)v_1' + u_1 + (2|u_1|^2 + |v_1|^2 + 2|u_3|^2 + 2|v_3|^2)v_1$$
$$+ v_1^{*2}v_3, \tag{A1b}$$

$$0 = 3\omega u_3 + i(1-\rho)u_3' + \Delta k u_3 + v_3 + 3(2|u_1|^2 + 2|v_1|^2 + |u_3|^2$$
$$+ 2|v_3|^2)u_3 + u_1^3, \tag{A1c}$$

$$0 = 3\omega v_3 - i(1+\rho)v_3' + \Delta k v_3 + u_3 + 3(2|u_1|^2 + 2|v_1|^2 + 2|u_3|^2$$
$$+ |v_3|^2)v_3 + v_1^3. \tag{A1d}$$

Numerical soliton solutions of the stationary equations were found by means of the relaxation technique [31]. [As an aside, the shooting method, which is a common alternative method for solving equations of this general nature, could not be implemented for Eqs. (A1) due to our lack of a measure of how "close" a guess is from a soliton solution.] We discretize the spatial axis and impose periodic boundary conditions (making sure, in the end, that a spatial extent of the resulting solutions is much smaller than the domain). This turns the ordinary differential equations for the functions u_1, u_3, v_1, v_3 into a set of finite-difference equations,

$$0 = \omega u_1^j + i(1-\rho)\frac{u_1^{j+1} - u_1^{j-1}}{2\Delta\zeta} + v_1^j + (|u_1^j|^2 + 2|v_1^j|^2 + 2|u_3^j|^2$$
$$+ 2|v_3^j|^2)u_1^j + (u_1^{j*})^2 u_3^j, \tag{A2a}$$

$$0 = \omega v_1^j - i(1+\rho)\frac{v_1^{j+1} - v_1^{j-1}}{2\Delta\zeta} + u_1^j + (2|u_1^j|^2 + |v_1^j|^2 + 2|u_3^j|^2$$

$$+ 2|v_3^j|^2)v_1^j + (v_1^{j*})^2 v_3^j, \tag{A2b}$$

$$0 = 3\omega u_3^j + i(1-\rho)\frac{u_3^{j+1} - u_3^{j-1}}{2\Delta\zeta} + \Delta k u_3^j + v_3^j + 3(2|u_1^j|^2 + 2|v_1^j|^2$$

$$+ |u_3^j|^2 + 2|v_3^j|^2)u_3^j + (u_1^j)^3, \tag{A2c}$$

$$0 = 3\omega v_3^j - i(1+\rho)\frac{v_3^{j+1} - v_3^{j-1}}{2\Delta\zeta} + \Delta k v_3^j + u_3^j + 3(2|u_1^j|^2 + 2|v_1^j|^2$$

$$+ 2|u_3^j|^2 + |v_3^j|^2)v_3^j + (v_1^j)^3, \tag{A2d}$$

where $\Delta\zeta$ is the transverse discretization step size, and j is the discrete coordinate on the grid. Finally, we use Newton's method [31] to obtain numerical solutions. Making initial guesses in Newton's method is a delicate process because the guess depends on many variables—the number of the spatial grid points times eight (as we are dealing with four complex variables). Our guesses were based on known solutions in various limits, with parameters altered. After obtaining particular solutions, nearby solutions were obtained by a continuation procedure, i.e., slightly changing the parameters and reapplying Newton's method, with the previous solution taken as the initial guess. We constructed families of solutions by evolving the numerical solutions in several dimensions of the parameter space: frequency (ω), velocity (ρ) [see Eqs. (6)], and phase-velocity mismatch (Δk). In this work, we do not present results obtained by varying other parameters, since they were found to be less critical for the soliton solutions than the set ($\omega, \rho, \Delta k$).

[1] W. Chen and D. L. Mills, Phys. Rev. Lett. **58**, 160 (1987).

[2] A. B. Aceves and S. Wabnitz, Phys. Lett. A **141**, 37 (1989).

[3] D. N. Christodoulides and R. I. Joseph, Phys. Rev. Lett. **62**, 1746 (1989).

[4] J. Feng, Opt. Lett. **18**, 1302 (1993); R. F. Nabiev, P. Yeh, and D. Botez, *ibid.* **18**, 1612 (1993).

[5] C. M. de Sterke and J. E. Sipe, Prog. Opt. **33**, 203 (1994); Adv. Mech. **3**, 384 (1998).

[6] A. B. Aceves, Chaos **10**, 584 (2002).

[7] G. P. Agrawal, *Nonlinear Fiber Optics* (Academic, San Diego, 1989).

[8] B. J. Eggleton, R. E. Slusher, C. M. de Sterke, P. A. Krug, and J. E. Sipe, Phys. Rev. Lett. **76**, 1627 (1996).

[9] B. J. Eggleton, C. M. de Sterke, and R. E. Slusher, J. Opt. Soc. Am. B **14**, 2980 (1997).

[10] D. Taverner, N. G. R. Broderick, D. J. Richardson, R. I. Laming, and M. Ibsen, Opt. Lett. **23**, 328 (1998).

[11] D. Mandelik, R. Morandotti, J. S. Aitchison, and Y. Silberberg, Phys. Rev. Lett. **92**, 093904 (2004).

[12] D. Neshev, A. A. Sukhorukov, B. Hanna, W. Krolikowski and Yu. S. Kivshar, Phys. Rev. Lett. **93**, 083905 (2004).

[13] T. Peschel, U. Peschel, F. Lederer, and B. A. Malomed, Phys. Rev. E **55**, 4730 (1997); C. Conti, S. Trillo, and G. Assanto, Opt. Express **3**, 389 (1998); Opt. Lett. **23**, 334 (1998).

[14] G. Kurizki, A. E. Kozhekin, T. Opatrny, and B. A. Malomed, Prog. Opt. **42**, 93 (2001).

[15] J. Atai and B. A. Malomed, Phys. Lett. A **155**, 247 (2001).

[16] A. A. Sukhorukov and Yu. S. Kivshar, Opt. Lett. **27**, 2112 (2002); I. M. Merhasin and B. A. Malomed, Phys. Lett. A **327**, 296 (2004).

[17] A. R. Champneys, B. A. Malomed, J. Yang, and D. J. Kaup, Physica D **152–153**, 340 (2001); W. C. K. Mak, P. L. Chu, and B. A. Malomed, J. Opt. Soc. Am. B **15**, 1685 (1998).

[18] Yu. S. Kivshar, Phys. Rev. E **51**, 1613 (1995); W. C. K. Mak, B. A. Malomed, and P. L. Chu, *ibid.* **58**, 6708 (1998).

[19] C. Etrich, F. Lederer, B. A. Malomed, T. Peschel, and U. Peschel, Prog. Opt. **41**, 483 (2000); A. V. Buryak, P. Di Trapani, D. V. Skryabin, and S. Trillo, Phys. Rep. **370**, 63 (2002).

[20] P. Di Trapani, D. Caironi, G. Valiulis, A. Dubietis, R. Danielius, and A. Piskarskas, Phys. Rev. Lett. **81**, 570 (1998).

[21] R. A. Sammut, A. V. Buryak, and Yu. S. Kivshar, Opt. Lett. **22**, 1385 (1997); J. Opt. Soc. Am. B **15**, 1488 (1998); K. Y. Kolossovski, A. V. Buryak, V. V. Steblina, A. R. Champneys, and R. A. Sammut, Phys. Rev. E **62**, 4309 (2000); V. C. Long, P. P. Goldstein, and M. Trippenbach, Acta Phys. Pol. A **105**, 437 (2004).

[22] C. V. Hile and W. L. Kath, J. Opt. Soc. Am. B **13**, 1135 (1996).

[23] P. Xie and Z.-Q. Zhang, Phys. Rev. E **71**, 026610 (2005).

[24] I. Bongrand, C. Montes, E. Picholle, J. Botineau, A. Picozzi, G. Cheval, and D. Bahloul, Opt. Lett. **26**, 1475 (2001).

[25] B. Shi, and X. Wang, Appl. Phys. Lett. **80**, 3667 (2002); M. G. Martemyanov, E. M. Kim, T. V. Dolgova, A. A. Fedyanin, O. A. Aktsipetrov, and G. Marowsky, Phys. Rev. B **70**, 073311 (2004).

[26] M. Trippenbach, M. Matuszewski, E. Infeld, C. L. Van, R. S. Tasgal, and Y. B. Band, Opt. Commun. **229**, 391 (2004).

[27] A. Gubeskys and B. A. Malomed, Eur. Phys. J. D **28**, 283 (2004).

[28] Y. Kodama and A. Hasegawa, IEEE J. Quantum Electron. **QE-23**, 510 (1987).

[29] R. W. Boyd, *Nonlinear Optics* (Academic, New York, 1992).

[30] R. S. Tasgal, M. Trippenbach, M. Matuszewski, and Y. B. Band, Phys. Rev. A **69**, 013809 (2004).

[31] W. H. Press, S. A. Teukolsky, W. T. Vetterling, and B. P. Flannery, *Numerical Recipes in Fortran 77* (Cambridge University Press, Cambridge, 2001).

[32] B. A. Malomed and R. S. Tasgal, Phys. Rev. E **49**, 5787 (1994).

[33] I. V. Barashenkov, D. E. Pelinovsky, and E. V. Zemlyanaya, Phys. Rev. Lett. **80**, 5117 (1998).

[34] M. K. Vakhitov and A. A. Kolokolov, Sov. J. Quantum Electron. **16**, 783 (1973); E. A. Kuznetsov, A. M. Rubenchik, and V. A. Zakharov, Phys. Rep. **142**, 103 (1986).